Global Biogeochemical Cycles

RESEARCH ARTICLE
10.1029/2021GB006977

Iron Isotope Biogeochemical Cycling in the Western Arctic Ocean

Ruifeng Zhang[1,2], Laramie Jensen[3], Jessica Fitzsimmons[3], Robert M. Sherrell[4], Phoebe Lam[5], Yang Xiang[5], and Seth John[2]

[1]School of Oceanography, Shanghai Jiao Tong University, Shanghai, China, [2]Department of Earth Sciences, University of Southern California Los Angeles, Los Angeles, CA, USA, [3]Department of Oceanography, Texas A&M University, College Station, TX, USA, [4]Department of Marine and Coastal Sciences and Department of Earth and Planetary Sciences, Rutgers University, New Brunswick, NJ, USA, [5]Department of Ocean Sciences, University of California Santa Cruz, Institute of Marine Sciences, Santa Cruz, CA, USA

Key Points:

- Sources and transport of Fe in the Western Arctic Ocean are well characterized by Fe stable isotopes during the U.S. GEOTRACES GN01 cruise
- δ^{56}Fe in shelf-modified Pacific water inflow indicates a sedimentary input of reduced Fe is laterally transported within Arctic halocline
- δ^{56}Fe in the Transpolar Drift Current averaged 0.02 ± 0.23‰, similar to the crustal average ratio and suggesting Fe input from Arctic rivers

Correspondence to:
R. Zhang,
ruifengzhang@sjtu.edu.cn

Citation:
Zhang, R., Jensen, L., Fitzsimmons, J., Sherrell, R. M., Lam, P., Xiang, Y., & John, S. (2021). Iron isotope biogeochemical cycling in the Western Arctic Ocean. *Global Biogeochemical Cycles*, *35*, e2021GB006977. https://doi.org/10.1029/2021GB006977

Received 13 FEB 2021
Accepted 19 OCT 2021

Abstract The Arctic Ocean is unique, connecting the Atlantic and Pacific basins and being especially vulnerable to the impacts of a changing climate. Iron stable isotopes (δ^{56}Fe) provide a unique window into the biogeochemical cycling of Fe in the Arctic. Here we present the first seawater δ^{56}Fe for the Western Arctic Ocean, from the 2015 U.S. GEOTRACES GN01 transect. Samples analyzed for δ^{56}Fe include seawater dissolved (<0.2 μm), soluble (<~0.003 μm), and leachable particulate phases. Several key processes were explored using Fe isotopes, each characterized by a distinct combination of δ^{56}Fe and Fe concentrations. Input of Fe from reducing continental shelf sediments was characterized by high dissolved Fe concentrations (6.18 ± 4.84 nmol kg^{-1}) and low δ^{56}Fe (−1.57 ± 0.66‰). Riverine Fe input observed in the Transpolar Drift Current was characterized by high Fe concentrations corresponding to a riverine end-member Fe concentration of 19 nM, and near-zero δ^{56}Fe (0.02 ± 0.23‰) that was similar to that of average crustal material. The deep Arctic was mostly characterized by low Fe concentrations (0.33 ± 0.14 nmol kg^{-1}) and slightly higher δ^{56}Fe (0.05 ± 0.30‰), except for samples taken near continental slopes that were affected by sedimentary Fe input with lower δ^{56}Fe, and in the Amundsen Basin which showed possible hydrothermal Fe input. Our data thus illuminate Fe biogeochemical cycling processes in the modern Arctic Ocean, and serve as a baseline for understanding how the Arctic Fe cycle responds to climate change.

1. Introduction

Iron is known as a key element that limits marine primary production in much of the ocean, due to its essential biological role and relatively low concentrations in the modern ocean (Martin, 1990; Moore et al., 2002). Thus, it is important to understand the external sources and sinks of Fe, its transport and cycling within the ocean, and how these both link to global biogeochemical processes and climate (Boyd & Ellwood, 2010; Tagliabue et al., 2017). Global efforts toward developing trace-metal clean sampling and analysis capabilities, along with inter-lab calibration efforts, have led to a surge in accurate Fe concentration data throughout the ocean (e.g., the international GEOTRACES program; R. Anderson, 2019). As a result of these new data, it is becoming increasingly possible to infer the sources and sinks of Fe in the ocean. Important iron sources include atmospheric deposition, riverine discharge, glacial meltwater inputs, sea ice, resuspension and oxic dissolution of sedimentary particles, input of reduced Fe(II) from anoxic sediments, and hydrothermal vents (Tagliabue et al., 2017, and references therein). Alongside Fe concentrations, Fe stable isotopes are a new tool to explore Fe cycling in the oceans, often elucidating sources, sinks, and mechanisms that cannot be constrained by iron concentrations alone. For example, Fe isotopes have been applied to trace the sources and transport of Fe to the ocean (Abadie et al., 2017; John et al., 2018; Labatut et al., 2014; Radic et al., 2011), to estimate the relative contribution of different iron sources to seawater (Conway & John,, 2014), and to study particular biogeochemical processes identified with particular isotope variations within single systems (Ellwood et al., 2015; Rouxel et al., 2016).

The Arctic Ocean is a particularly important place to study Fe biogeochemistry because of the disproportionately high continental margin and riverine sources and because of the potential role of Fe as a critical micronutrient for phytoplankton. In comparison to other oceans, the Arctic receives the most riverine

input, contains the largest relative continental shelf area, and is the only basin largely covered with seasonal and multi-year ice (Carmack, 2007). Over the past decade, the Arctic has been warming at more than twice the global mean rate (Overland et al., 2019), and thus the Arctic Ocean is experiencing the effects of climate change at a rate faster than most other places on Earth. Consequences of this warming include accelerated melting of glaciers, freshening of Arctic surface waters, decreasing sea ice cover, and increasing stratification (Manizza et al., 2019; Post et al., 2013). In the rapidly changing Arctic Ocean, trends in marine primary productivity are influenced by both light and nutrient limitation (Lewis et al., 2019; Schourup-Kristensen et al., 2018). Although nitrate is thought to currently be the main limiting nutrient in the Arctic Ocean (Granger et al., 2018), iron may play a larger role limiting productivity in the future (Taylor et al., 2013), as it does in other high-latitude regions including the Southern Ocean and the subarctic North Pacific. For example, some Eastern Arctic subsurface waters are stoichiometrically Fe-limited, and Fe could limit up to half of the available nitrogen from being consumed by primary producers (Rijkenberg et al., 2018). However, the freshening Arctic might be expected to decrease nitrogen supply to the surface relative to Fe, and thus trends in future primary production may be interpreted largely in terms of N availability (Randelhoff et al., 2020). Or, nutrient supply of Fe and N might have interactive effects. There is evidence that marine nitrogen fixation could be an important source of nitrogen to the seasonally nitrogen-limited Arctic Ocean (Harding et al., 2018; Sipler et al., 2017). Because of the large requirement of iron by marine nitrogen fixing organisms (Berman-Frank et al., 2007), the generally high Fe flux into Arctic surface waters may fuel the biological fixed nitrogen and support marine primary production in Arctic. It is therefore crucial to study the biogeochemical cycling of Fe as part of the overall effort to understand how nutrient cycling and biological productivity will change in a warming Arctic.

Previous studies have examined Fe sources to the Arctic, and their transport throughout the Arctic Ocean. Both Atlantic and Pacific waters enter the Arctic Ocean, bringing Fe with them. Within the Arctic, rivers are also an important source of Fe (Charette et al., 2020; Klunder, Bauch, et al., 2012). Riverine Fe has been suggested to be complexed by humic substances (Slagter et al., 2017, 2019), and transported into the central Arctic basin along the transpolar drift (TPD) (Laglera et al., 2019), a process recently explored using a wide spectrum of evidence including δ^{56}Fe (Charette et al., 2020). Other potential surface sources of Fe include melted sea ice (Aguilar-Islas et al., 2008; Evans & Nishioka, 2018; Measures, 1999) and melting icebergs and glacial meltwater (Hopwood et al., 2017). In the subsurface Arctic, lateral Fe transport from the Chukchi Shelf is thought to be an important Fe source to the Arctic (Aguilar-Islas et al., 2013; Cid et al., 2012; Klunder, Laan, et al., 2012), with the shelf Fe originating from porewater Fe(II) inputs (Vieira et al., 2019), and then being stabilized for transport into the open Arctic ocean by complexation with humic-like dissolved organic matter (Hioki et al., 2014). Transport time of halocline waters from the shelf to the Arctic basin interior is greater than 30 years, with Fe eventually reaching the surface through vertical mixing (Kipp et al., 2019). In the deeper Arctic Ocean, both seafloor sediments and hydrothermal vents can be important sources of Fe (Klunder, Bauch, et al., 2012; Valk et al., 2018). Aerosol inputs to the Arctic are small, and the residence time of dissolved Fe (dFe) in surface water with respect to atmospheric deposition is estimated at around 20–40 years (Kadko et al., 2019). In the future, land areas around the Arctic Ocean that are impacted by freeze-thaw cycles and precipitation could become increasingly important summertime sources of aerosol Fe (Gao et al., 2019). The sinks by which Fe is lost from the Arctic may include biological uptake at the surface, particle scavenging within the water column, and ferromanganese oxide formation and deposition (Hein et al., 2017; Jensen, Morton, et al., 2020; Klunder, Laan, et al., 2012; Vieira et al., 2019).

Prior iron isotope data from the Arctic region has focused on riverine and glacial inputs. The δ^{56}Fe values in a glacial meltwater stream on Svalbard ranged between −0.11‰ and +0.09‰ (Zhang et al., 2015), and the isotopic signature of dFe was also found to be similar to crustal values in a glacier-fed tributary of the Copper River (Schroth et al., 2011). Although, a recent study has suggested that subglacial streams which are subjected to incongruent silicate weathering and sulfide oxidation may supply Fe with a low δ^{56}Fe signature down to −2.1‰ (Stevenson et al., 2017). The Fe isotopic composition of large Arctic rivers has a restricted range of δ^{56}Fe values (−0.11‰ to 0.13‰) with low seasonal variability (Escoube et al., 2015). Slight differences in riverine particulate δ^{56}Fe were observed between particles (>0.22 μm) and colloids in the Lena River (Hirst et al., 2020). After modification in the Lena River estuary, positive δ^{56}Fe values (around +0.10‰) were observed in the outermost stations of the East Siberian Arctic Shelf (Conrad et al., 2018). Taken together, these previous studies suggest that the δ^{56}Fe fingerprint of Arctic rivers is close to the mean

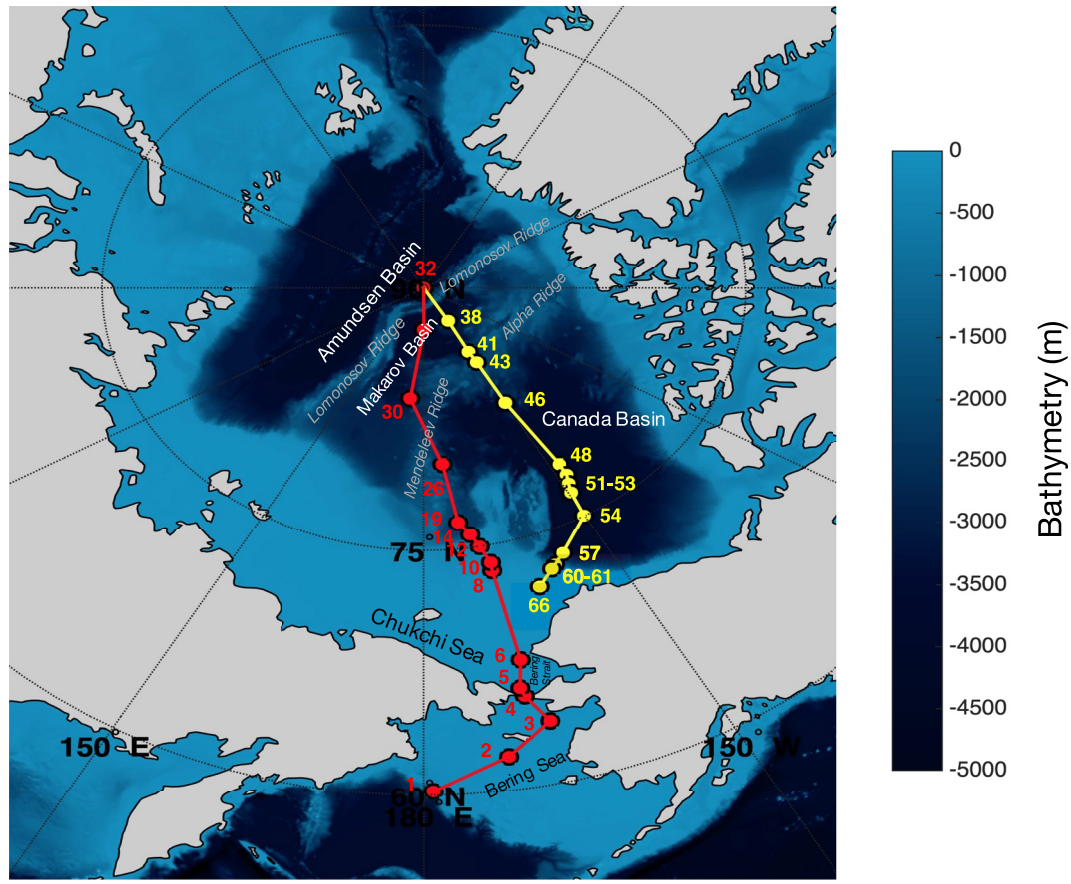

Figure 1. Station map for the US GEOTRACES GN01 cruise track in the Western Arctic Ocean. The cruise track in red represent the northward transect from the North Pacific, via the Bering Sea, Bering Strait, Chukchi Sea, and the northward across the Canada and Makarov Basins to the North Pole. The returning southward track is shown by the yellow line crossing back across the Makarov and Canada Basins, and ending on the Chukchi Shelf.

terrigenous crustal ratio (+0.09‰, Beard et al., 2003). A recent study of snow sampled during the US GEOTRACES GN01 Arctic cruise found δ^{56}Fe values in snow (−0.61‰ to −0.38‰) and sea ice (−1.10‰ to −0.17‰) which were lighter than the crustal ratio and mostly lighter than underlying seawaters, suggesting active Fe cycling within the cryosphere (Marsay et al., 2018).

In this study, we present the first comprehensive study of seawater Fe isotopes in the Arctic Ocean, including soluble (<10 kDa; ~0.003 μm), dissolved (<0.2 μm), and leachable particulate phases, for samples collected in the Western Arctic Ocean during the 2015 U.S. GEOTRACES GN01 cruise. Samples were collected for full depth water profiles at 28 stations, and 8 of these profiles were sampled for soluble Fe. 20 particle profiles were taken for labile 'ligand-leachable' particulate Fe isotope analysis. These data provide information about the sources and sinks of Fe in the Arctic Ocean, as well as about important internal biogeochemical cycling processes.

2. Methods

2.1. Cruise Information

The U.S. GEOTRACES GN01 cruise was carried out on USCGC *Healy* (cruise HLY1502) during late summer 2015, departing Dutch Harbor, Alaska, on August 9, 2015 and returning to Dutch Harbor on October 12, 2015. The Arctic Ocean is divided into the Amundsen Basin and the Amerasian Basin by the Lomonosov Ridge (Figure 1). The Alpha and Mendeleev Ridges separate the Amerasian Basin into the Makarov Basin and the Canada Basin. The cruise track consisted of a northward transect from the North Pacific, via the

Bering Sea, Bering Strait, Chukchi Sea, and northward across the Canada and Makarov Basins to the North Pole, returning southward back across the Makarov and Canada Basins, and ending on the Chukchi Shelf (Figure 1). A total of 28 trace metal clean full water column stations, and 20 trace metal particle profiles were sampled, and dissolved phase Fe isotopes were analyzed at all stations.

Nutrient and hydrographic data (e.g., salinity, temperature, and dissolved oxygen) were analyzed at the Scripps Oceanographic Data Facility using standard methods, and data are available on the Biological and Chemical Oceanography Data Management Office (BCO-DMO) website (https://www.bco-dmo.org/deployment/638807). Data are plotted using an in-house Matlab routine which first linearly interpolates data at each station in the vertical direction, then interpolates horizontally between stations.

2.2. Sampling and Sample Handling for Dissolved, Soluble, and Particulate Phases

Seawater samples were collected by deploying a trace-metal clean CTD/rosette attached to a plastic-coated hydrowire and fitted with 12-L Teflon-coated GO-Flo bottles, and then filtered through AcroPak-200 Supor cartridges (0.8/0.2 μm polysulfone membrane; Pall) into pre-acid-cleaned 1 L low-density polyethylene (LDPE, Nalgene) bottles by the GEOTRACES sampling team (Cutter & Bruland, 2012). In addition to GO-Flo samples, near surface seawater samples were collected at 1, 5, and 20 m below the ice using a battery powered peristaltic pump (Pegasus Alexis) with an acid cleaned fluorinated ethylene propylene (FEP)-lined Tygon tubing (Cole Parmer). Under-ice samples were pumped under the protection of a tent into a 25 L acid cleaned polyethylene carboy, and were subsequently subsampled into clean 1 L LDPE bottles. At eight stations, additional samples were collected for size-fractionation analyses and subjected to cross-flow filtration (10 kDa; ~0.003 μm assuming globular proteins). Ultrafiltration was operated in a positive pressure "clean bubble" within 3 h of collection to prevent bottle effects (Fitzsimmons & Boyle, 2014; Jensen, Wyatt, et al., 2020). Thus, the dissolved samples for trace metal analysis allow us to distinguish metals in the soluble (<0.003 μm), colloidal (0.003–0.20 μm), and dissolved (<0.2 μm) phases, though only dissolved and soluble phases are measured directly, and the composition of the colloidal phase is calculated as the difference between the dissolved and soluble. Suspended particles (0.8–51 μm) were sampled from up to 24 depths at 20 stations with McLane in situ pumps (Ohnemus & Lam, 2015; Xiang & Lam, 2020). Samples for trace metal analyses were collected on paired 142 mm diameter 0.8 μm polyethersulfone (Supor) filters loaded underneath a 51 μm polyester mesh prefilter, through which 100–500 L of seawater were typically pumped (Bishop et al., 2012; Lam et al., 2018; Lee et al., 2018; Xiang & Lam, 2020).

2.3. Fe and Fe Isotope Analysis for Soluble and Dissolved Phases

Prior to processing large-volume samples, all samples were analyzed for Fe concentrations at both USC and Texas A&M with an isotope dilution offline seaFAST pico method (Elemental Scientific Incorporated), to optimize the isotopic ratio for δ^{56}Fe analysis (Jensen, Morton, et al., 2020). Seawater for soluble Fe (sFe) and dissolved Fe (dFe) phases was then processed and analyzed at the University of Southern California for Fe concentrations and δ^{56}Fe according to previously published methods (Conway et al., 2013). In brief, 1 L samples were acidified with HCl to pH ~ 1.7 in a class-100 laminar clean flow bench in a clean lab and stored at room temperature for several months before being processed. Samples were then amended with a ~1:1 57Fe-^{58}Fe double spike, and left to equilibrate for at least 2 hr before extraction. Iron was extracted by bulk extraction onto Nobias chelating resin PA-1. Fe was then eluted from the Nobias resin with 3 M sub-boiling Teflon-distilled HNO_3 and purified by anion exchange chromatography. Finally, samples were analyzed for Fe concentration and δ^{56}Fe on a Neptune multi collector Inductively Coupled Plasma Mass Spectrometry (ICPMS) at the California Institute of Technology, with δ^{56}Fe reported relative to IRMM-014. The typical 2σ analytical error is less than 0.05‰. Fe concentrations were calculated by isotope dilution, and converted to nmol kg^{-1} using the weight of each sample processed, as described in previous work (Conway et al., 2013; Jensen, Morton, et al., 2020). The fraction of colloidal Fe (%cFe) was calculated by dividing the inferred colloidal Fe concentration by the measured total dissolved Fe concentration.

Fe concentration data reported in this manuscript are from 1 L samples processed at USC, which agree well with analyses performed TAMU (Figure 2).

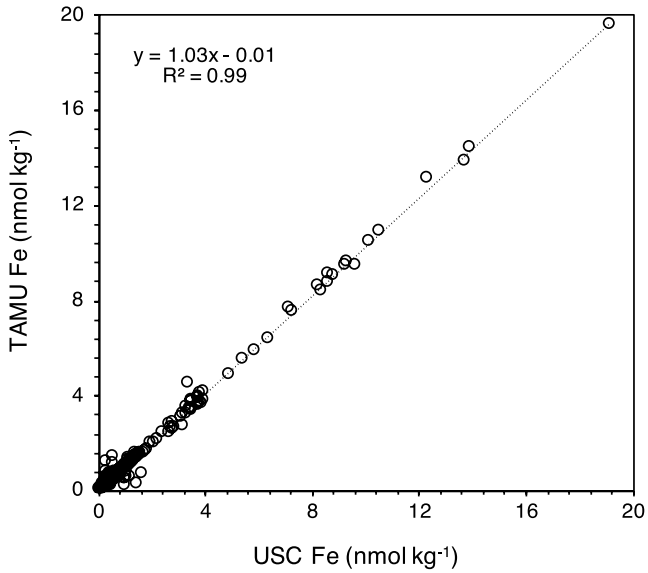

Figure 2. Iron concentrations measured at Texas A&M University (TAMU) (Jensen, Morton, et al., 2020) compared to those for samples processed at the University of Southern California (USC). The solid line reflects the mean relationship between the data sets.

2.4. Fe and Fe Isotope Analysis for Leachable Particulate Phase

A clean pH eight oxalate-EDTA leach solution was prepared to extract "ligand-leachable" Fe from marine particles (Revels et al., 2015). Each filter section was folded loosely and sealed in a 2 mL polyethylene vial (Nalgene) with 1 mL of oxalate-EDTA leach solution and heated at 90 °C for 2 hr. The leachate was then transferred into a 3 mL polypropylene syringe (Norm-Ject) and filtered with a 0.45 μm PTFE membrane (Whatman). Multi-element concentrations were analyzed on an Element two ICPMS at USC by diluting the leachate to 5% of the original concentration with 0.1 M HNO_3, and measuring signal intensity relative to standards in the same combination of reagents. About 10 ppb In was added to all samples, blanks, and standards as an internal standard. Following the method described by Revels et al. (2015), aliquots of each leachate, typically containing ~75 ng of Fe, were transferred to 7 mL Teflon PFA vials. Samples were then spiked with a ~1:1 57Fe-^{58}Fe double spike, to yield a 1:2 natural-to-spike Fe ratio. The spiked samples were evaporated to dryness, and then reacted with mixture of HNO_3 and H_2O_2 at 200°C for 2.5 h to digest organic material in the leachate. After being brought to dryness for a second time, samples were reconstituted in 10 M HCl with 0.01% v/v H_2O_2 and purified by anion exchange chromatography. Samples were then dried down and reconstituted in 1.5 mL of 0.1 M HNO_3 for isotopic analysis. The batch of oxalate EDTA leach solution contained an Fe concentration of 8.52 ± 0.06 ng g^{-1}, with δ^{56}Fe of −3.46 ± 0.10‰ (mean ± 1σ, n = 4). The oxalate EDTA leach solution contributed ~10% of the overall analytical blank, such that the uncertainty within the leach solution contributed less than 3% of the overall analytical variance. Final values of leachable particulate Fe concentrations and δ^{56}Fe were reported after blank correction.

The fraction of labile particulate Fe (f_{labile}Fe) was calculated as the leachable particulate Fe concentration divided by the total particulate Fe concentration. The detailed procedures and analysis for total particulate Fe concentration are described in Xiang and Lam (2020), which are an adaptation of the method used by Planquette and Sherrell (2012) and intercalibrated in Ohnemus et al. (2014). In brief, the particulate filters were cut into small pieces, and refluxed in a 50% HNO_3/10%HF mixture at 110 °C. After digestion, samples were re-dissolved in 5% HNO_3 and analyzed for Fe using an Element XR ICPMS at University of California, Santa Cruz.

3. Results

Based on prior literature and observed biogeochemical features (Figure 3), we have defined four distinct Arctic water masses by salinity (Zhang et al., 2019, and the references therein): Arctic surface water (SW; Salinity <30.70), halocline (HC; Salinity 30.70–34.80), Atlantic water (AW; Salinity 34.80–34.92), and Arctic deep water (DW; Salinity >34.92), from surface to bottom, respectively. Station 1 was located in the North Pacific (designated PAC), while Stations 2–8 and 61–66 were located over the Bering or Chukchi shelf (designated SHELF). Briefly, these water masses have several important key features. Surface seawater has low salinity SW (approximately the upper 50 m) with low nutrient concentrations as seen in dissolved silicate concentrations (Figure 3c). HC waters—characterized by high nutrient concentrations, low dissolved oxygen, and low temperature—originate as Pacific waters that cross the Bering/Chukchi Shelves, where they may become enriched by sediment fluxes (e.g., Zn: Jensen et al., 2019) and are further modified by brine rejection during sea ice formation. Both AW and DW originate in the North Atlantic, and both have relatively high-salinity and are warmer than waters originating in the Pacific; they are distinguished from each other by the slightly higher silicate (Si) concentrations observed in DW. While water-mass characteristics are generally similar for each of these water types, it should be noted that surface waters (SW) include both near-shelf waters which appear to be more influenced by processes near the Bering and Chukchi shelves,

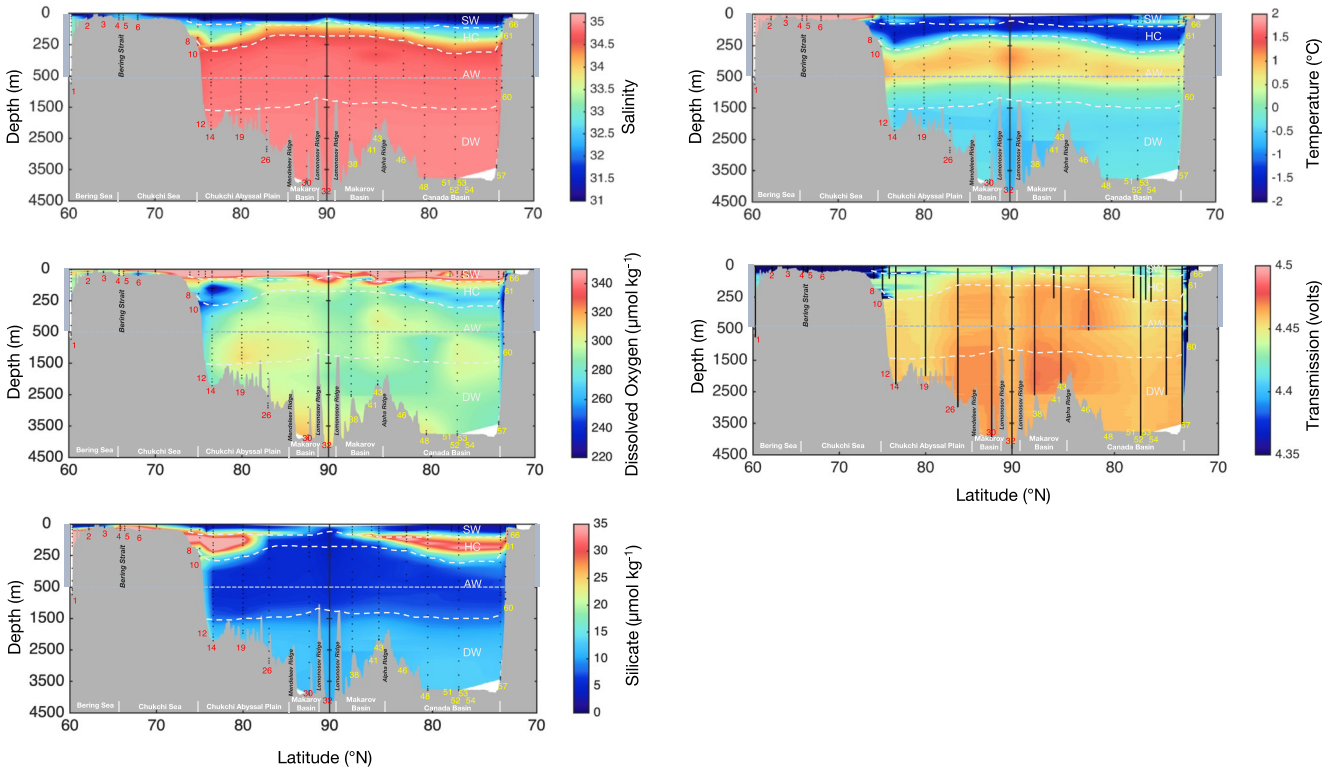

Figure 3. Salinity, temperature, dissolved oxygen, transmission, silicate distributions along the US GEOTRACES GN01 cruise in the Western Arctic. Four water masses in the Western Arctic ocean were identified, including SW: surface water, HC: Halocline, AW: Atlantic layer water, DW: deep Arctic water. The upper 500 m is expanded to show detailed characteristics in surface waters and the halocline.

and waters near the North Pole which are more influenced by inputs along the Siberian Shelf, carried to the polar region with the Transpolar Drift (TPD) (Charette et al., 2020).

3.1. Spatial Distribution of Fe and δ^{56}Fe in Different Phases

Clear patterns were observed in the concentration distributions and δ^{56}Fe of dissolved Fe (dFe), soluble Fe (sFe), and leachable particulate Fe (lpFe) during the GN01 cruise (Figure 4). Within the single North Pacific station (PAC), low dFe concentrations were observed from the surface to 175 m, ranging from 0.04 to 0.30 nmol kg^{-1}, with associated δ^{56}Fe from −0.14‰ to −1.07‰. Iron concentrations increased with depth, with dFe between 1.00 and 1.54 nmol kg^{-1} from 249 to 733 m, and the associated δ^{56}Fe was lighter, from −0.90‰ to −1.49‰ (sFe not sampled at PAC). At the PAC site, lpFe concentrations averaged 0.81 ± 1.07 nmol kg^{-1} (n = 4) with a maximum of 2.41 nmol kg^{-1} at 274 m, and average δ^{56}Fe values of −0.31 ± 0.28‰ (n = 4).

Concentrations of all three Fe species were quite high on the Bering Shelf and Chukchi Shelf (SHELF), averaging 6.2 ± 4.8 nmol kg^{-1} dFe (n = 31), 4.6 ± 3.1 nmol kg^{-1} sFe (n = 7), and 170 ± 188 nmol kg^{-1} lpFe (n = 12). Iron isotopes were lighter than continental material, with dissolved δ^{56}Fe, soluble δ^{56}Fe and leachable particulate δ^{56}Fe, averaging −1.6 ± 0.7‰ (n = 31), −1.1 ± 0.3‰ (n = 7), and −1.0 ± 0.3‰ (n = 12), respectively.

Within the four different Arctic Ocean water masses (SW, HC, AW, and DW), we observed large variations in both the concentrations and δ^{56}Fe of all the Fe phases. Concentrations of dFe ranged from 0.17 to 5.81 nmol kg^{-1}, sFe ranged from 0.10 to 1.89 nmol kg^{-1}, and lpFe ranged from 0.06 to 90.15 nmol kg^{-1}, respectively. Fe isotope values (δ^{56}Fe) of dissolved, soluble, and leachable particulate Fe ranged from −1.68‰ to +0.85‰, from −1.88‰ to +0.62‰, and from −1.41‰ to +0.28‰, respectively.

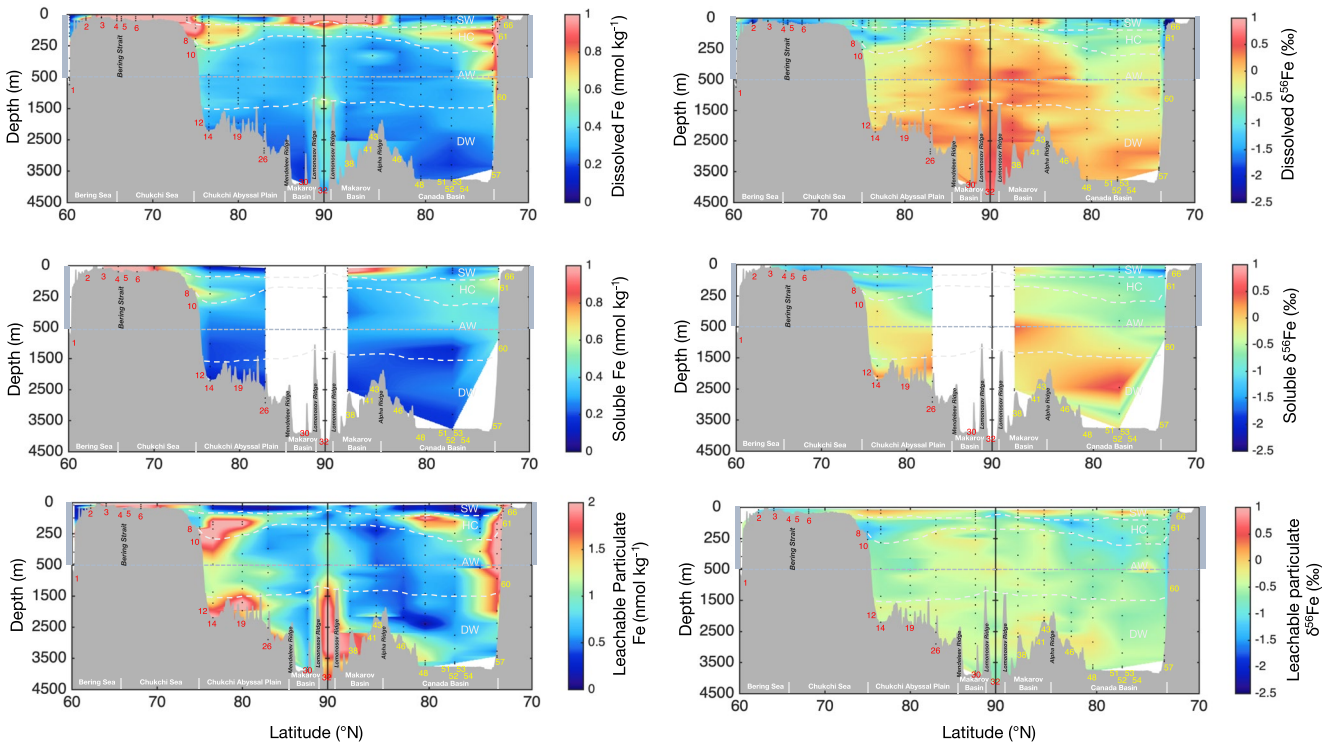

Figure 4. Dissolved Fe concentration, dissolved δ^{56}Fe, soluble Fe (<10 kDa) concentration, soluble δ^{56}Fe, leachable particulate Fe concentration, leachable particulate δ^{56}Fe distributions along the U.S. GEOTRACES GN01 cruise.

In the Arctic SW, dissolved δ^{56}Fe highlights two different regimes. In the more southerly stations nearer to the continental shelves, dFe was relatively low (averaging 0.34 ± 0.28 nmol kg^{-1}, n = 41) and the dissolved Fe was isotopically lighter (−1.02 ± 0.32‰, n = 41). In contrast, for the more northerly stations near the North Pole (stations 30–43), Fe concentrations were notably higher (3.14 ± 0.97 nmol kg^{-1}, n = 23) and the Fe isotopes were heavier (δ^{56}Fe = 0.02 ± 0.23‰, n = 23). Similarly, a single sample at Station 38 was observed with higher concentration of 1.89 nmol kg^{-1} and heavier isotopic ratio of 0.27‰ in soluble phase, compared to 0.25 ± 0.15 nmol kg^{-1} and −1.15 ± 0.42‰ (n = 15) near the continental shelves. However, with few data points, patterns for leachable particulate Fe were indistinguishable between the two regimes, lpFe = 0.50 ± 0.39 nmol kg^{-1} and lpδ^{56}Fe = −0.09 ± 0.33‰ (n = 4) near the North Pole, lpFe = 0.43 ± 0.45 and lpδ^{56}Fe = −0.14 ± 0.30‰ (n = 8) in the southernly stations, respectively.

In the halocline (HC) waters, Fe and δ^{56}Fe had similar patterns in all three phases, with high Fe concentrations and low δ^{56}Fe for dFe, sFe, and lpFe, averaging 0.70 ± 0.53 nmol kg^{-1} and −0.56 ± 0.43‰ (n = 92), 0.46 ± 0.34 nmol kg^{-1} and −0.74 ± 0.47‰ (n = 16), 7.33 ± 28.98 nmol kg^{-1} and −0.76 ± 0.36‰ (n = 56), respectively. The vertical extent of the HC waters decreases toward the North Pole, and patterns of Fe distribution followed this same pattern, although with increasing distance from the shelf, Fe concentrations decreased and δ^{56}Fe increased.

In Arctic AW and DW water masses, Fe concentrations were generally low and δ^{56}Fe signatures were heavier. The averaged dFe concentrations were 0.38 ± 0.16 nmol kg^{-1} (n = 90) and 0.27 ± 0.07 nmol kg^{-1} (n = 67), in AW and DW, respectively. The averaged dissolved δ^{56}Fe were −0.03 ± 0.31‰ (n = 90), and +0.16 ± 0.26‰ (n = 67), in AW and DW, respectively. For the single station which sampled the Amerasian Basin, at the North Pole below 1,500 m, both dFe and lpFe concentrations were higher, averaging 0.41 ± 0.08 nmol kg^{-1} and 2.10 ± 0.48 nmol kg^{-1}, respectively.

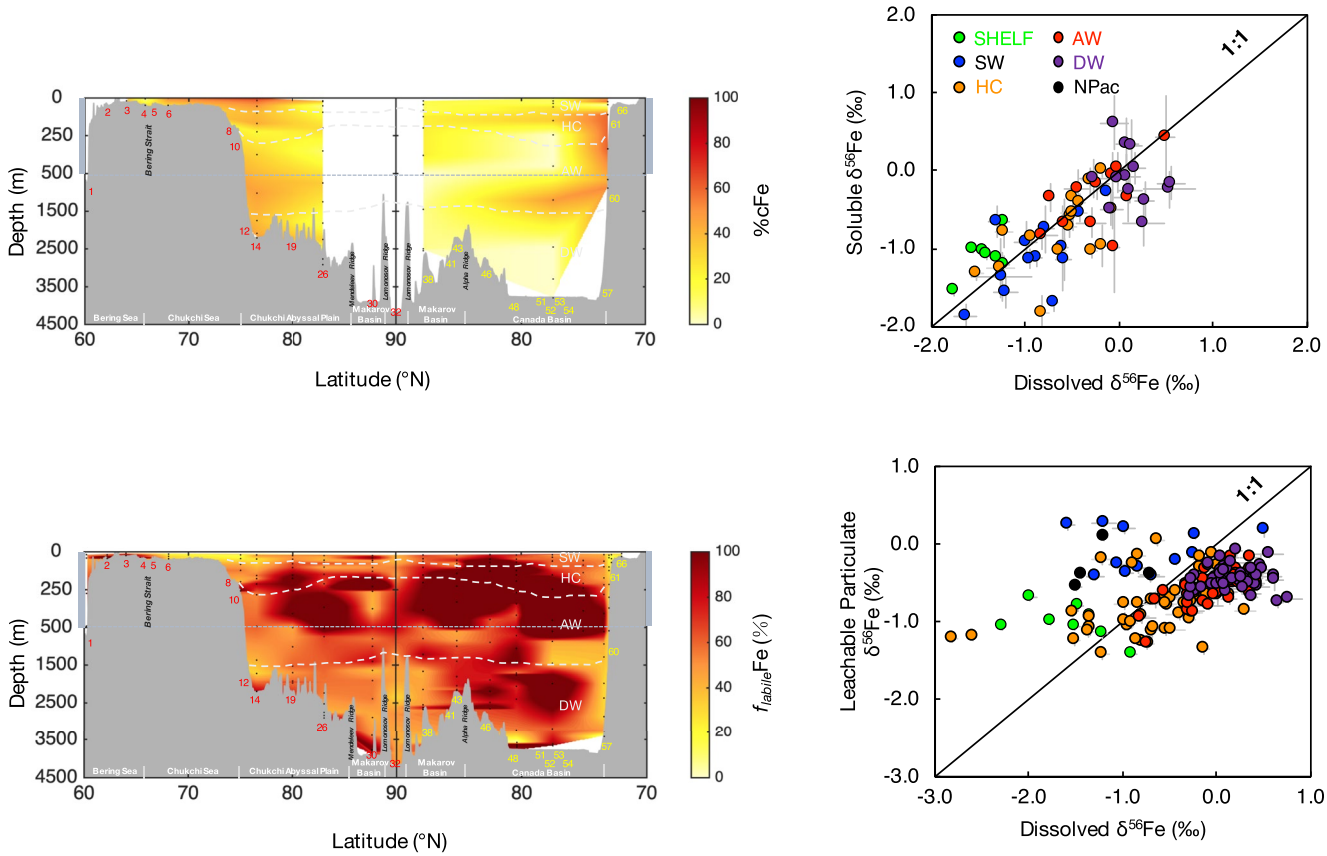

Figure 5. Fraction of colloidal Fe (<10 kDa - 0.20 μm) (a), fraction of labile particulate Fe distribution in the Western Arctic Ocean (b), the relationship between soluble δ^{56}Fe and dissolved δ^{56}Fe (c), and the relationship between leachable particulate δ^{56}Fe and dissolved δ^{56}Fe (d).

3.2. Correlation Between Soluble δ^{56}Fe and Dissolved δ^{56}Fe, Leachable Particulate δ^{56}Fe and Dissolved δ^{56}Fe

The fraction of dissolved Fe found in the colloidal size-class (%cFe) ranged from 0% to 81%, with an average value of 30 ± 21% over the entire GEOTRACES GN01 transect. Higher %cFe was typically found above the continental shelves and in surface waters (Figure 5), which is similar to prior studies of dissolved Fe size partitioning in the presence of external Fe fluxes such as dust or margin fluxes (Bergquist et al., 2007; Fitzsimmons, Carrasco, et al., 2015; Fitzsimmons, Hayes, et al., 2015; Jensen, Morton, et al., 2020). The distribution pattern of dissolved δ^{56}Fe is similar to that of soluble δ^{56}Fe, which is obviously due to the fact that soluble Fe dominated the dissolved phase during the GN01 cruise. This is similar to the only other published soluble δ^{56}Fe values from the GEOTRACES GA03 subtropical North Atlantic section (Fitzsimmons, Carrasco, et al., 2015), where soluble and dissolved δ^{56}Fe were identical in subsurface waters, but in surface waters soluble δ^{56}Fe was significantly heavier than dissolved and calculated colloidal δ^{56}Fe. Similarly, in the Arctic, all measured soluble δ^{56}Fe in SHELF stations (−1.09 ± 0.27‰) was significantly heavier (ANOVA, $p = 0.026$) than dissolved δ^{56}Fe (−1.57 ± 0.66‰), requiring an isotopically lighter colloidal-phase δ^{56}Fe. This supports the hypothesis of Fitzsimmons, Carrasco, et al. (2015) that isotopically heavier soluble δ^{56}Fe is formed by the binding of smaller soluble Fe by very strong ligands (Dideriksen et al., 2008; Morgan et al., 2010), including but not limited to siderophores.

For particle samples, values of f_{labile}Fe ranged from less than 1% (bottom water at Station 57) to >100%. Lower fractions of labile Fe were most often found over the continental shelf and close to the continental slope, suggesting refractory lithogenic particle input. The range of ligand-leachable particulate δ^{56}Fe was narrower compared to that of dissolved δ^{56}Fe. There was often a co-occurrence of lighter dissolved δ^{56}Fe and lighter ligand-leachable particulate δ^{56}Fe (Figure 5).

4. Discussion

The Arctic connects the Pacific and the Atlantic oceans. Pacific waters flow into the Arctic through the shallow Bering Strait, and there is strong seasonal variability to this input (Woodgate, 2013). The inflowing Pacific water sinks below fresher SW formed by brine rejection from sea ice, to form a halocline water mass with high nutrient concentrations derived from the Pacific source water. These upper halocline waters are mostly found in the Western Arctic, closer to the Pacific inflow. The Atlantic water inflow enters through both the Fram Strait and the Barents Sea to form the relatively homogenous Arctic AW (Woodgate, 2013). The Fram Stait is the only passage which permits DW exchange (Rudels et al., 1991).

Geochemical parameters, including trace metals, are good tracers for these ocean circulation patterns and water masses. Similar to patterns in hydrology, macronutrients, and other geochemical tracer distributions that have been reported previously (e.g., Jensen et al., 2019; Kipp et al., 2019; Whitmore et al., 2019; Zhang et al., 2019), Fe and Fe stable isotopes reflect a general basin-scale mixing between Atlantic and Pacific waters (Figures 3 and 4). Broadly speaking, we observed four different sources of Fe into the Arctic Ocean based on the concentration and Fe stable isotope ratios observed in the dissolved, soluble, and leachable particulate phases. These include (a) riverine Fe input along the Siberian Shelf leading to high Fe concentrations and near-zero δ^{56}Fe near the North Pole in the region impacted by the transpolar drift, (b) Fe input from reducing sediments on the continental shelf impart Pacific inflow waters with high dFe and low δ^{56}Fe, which are subsequently transported laterally along the halocline into the Arctic, (c) inflow from the Atlantic Ocean dominates the deep Arctic with relatively low dFe and higher δ^{56}Fe, and (d) deviations from the otherwise homogeneous deep Arctic dFe and δ^{56}Fe resulting from sedimentary inputs near the continental slope and hydrothermal Fe inputs in the Amundsen Basin.

4.1. Fe in the Transpolar Drift

The Western Arctic is characterized by a cold and fresh surface mixed layer (Anderson et al., 2013). Circulation within the surface ocean is dominated by two major features: the anticyclonic Beaufort Gyre in the Canada Basin (which spanned from roughly 75°N to 85°N on GN01) and the transpolar drift (TPD) which crosses the Arctic Basin from the East Siberian and Laptev Seas to the Fram Strait and was transected by GN01 between 85°N and the North Pole (Charette et al., 2020). Arctic river runoff contributes about two thirds of the freshwater budget in the TPD (Woodgate, 2013) and is an important source of terrestrial materials into the Arctic. Previous studies have noted the input of various riverine constituents with the TPD including dissolved organic matter, radium isotopes, Ba and Co (Bundy et al., 2020; Charette et al., 2020; Guay & Kenison Falkner, 1997; Kipp et al., 2018; Rutgers van der Loeff et al., 2018; Shen et al., 2016; Slagter et al., 2019). Using pan-Arctic data from this GN01, the Eastern Arctic GN04 and the Fram Strait GN05 study that crossed the TPD in 2015, it was reported that the TPD carried elevated dissolved Fe and Fe-binding ligand concentrations compared to the rest of the Arctic, composed mostly of smaller soluble-sized compounds (Ardiningsih et al., 2020; Charette et al., 2020; Krisch et al., 2020). The δ^{56}Fe signatures of this dissolved Fe were near zero, unique for the otherwise isotopically light surface Arctic waters, and indicative of riverine Fe inputs (Charette et al., 2020). It has also been reported that TPD waters contain elevated concentrations of Fe-binding ligands (Slagter et al., 2017), including especially humic compounds (Slagter et al., 2019).

The elevated dissolved Fe concentrations within the transpolar drift, along with δ^{56}Fe signatures near zero, are both easily distinguishable from underlying waters and more southerly Beaufort Gyre surface waters in section space (Figure 5). The location of TPD waters on GN01 (Stations 30–43, down to 80 m depth) was determined primarily from the fraction of seawater derived from meteoric water sources (river and precipitation, quantified by δ^{18}O, Charette et al., 2020). Within these TPD waters, dFe averaged 3.14 ± 0.97 nmol kg^{-1} (n = 23) which is similar to values reported previously in the TPD by (Klunder, Bauch, et al., 2012) and Rijkenberg et al. (2018). Dissolved δ^{56}Fe in TPD waters was 0.02 ± 0.23‰ (n = 23). This value is distinct from the much lower δ^{56}Fe values typically seen for Fe input from reducing sediments on continental shelves (−2‰ to −4‰; John et al., 2012, 2018; Severmann et al., 2010), and from the lower δ^{56}Fe observed in adjacent waters on this transect. Thus, we corroborate that Fe in the TPD most likely has a riverine origin.

The near-zero δ^{56}Fe observed in the TPD is consistent with many observations of Arctic rivers in both the dissolved and colloidal phase (Conrad et al., 2019; Escoube et al., 2015; Hirst et al., 2020; Schroth et al., 2011), as well as values measured for glacial meltwaters (Zhang et al., 2015). Stevenson et al. (2017) observed negative δ^{56}Fe values from some subglacial meltwater in Greenland. Their results also showed that more mature subglacial systems have dissolved loads with δ^{56}Fe close to zero. The constraint on iron isotope signatures from glaciers depends on the bedrock types, weathering conditions, proglacial environment and the fate after mixed with seawaters, all of which require further study. The average δ^{56}Fe for rivers throughout the Arctic is −0.11 ± 0.27‰, including data from the Ob and Lena (Conrad et al., 2019; Escoube et al., 2015) and the Copper River (Schroth et al., 2011). Dissolved Fe in the TPD exhibited a strong correlation with the fraction of meteoric water (R^2 = 0.67) (Charette et al., 2020), with this correlation pointing to a freshwater endmember of 19 nmol kg^{-1}. This Fe concentration is less than 1% of dFe measured in the Ob and Lena Rivers (Escoube et al., 2015; Holmes et al., 2012), corroborating that most riverine Fe is lost during estuarine mixing (Boyle et al., 1977; Dai & Martin, 1995). The fact that δ^{56}Fe in the TPD matches that of Arctic rivers, within error, suggests that there is little chemical or biological cycling of Fe during estuarine mixing and transport into the central Arctic. Instead, Fe is most likely lost by a non-fractionating process such as the coagulation and adsorption of colloidal Fe or humic-bound Fe, as previously observed in Arctic glacial rivers (Zhang et al., 2015) and other non-Arctic estuarine systems (e.g., Boyle et al., 1977; Escoube et al., 2015).

Other Fe phases also have near-zero δ^{56}Fe in the TPD. Only two soluble Fe samples were taken in the TPD (Station 38) with δ^{56}Fe values of −0.27‰ and +0.01‰ at 19 and 44 m, respectively, compared to total dissolved phase δ^{56}Fe in these same samples of −0.12‰ and −0.17‰. Six labile particulate δ^{56}Fe samples averaged −0.2 ± 0.3‰ in the TPD, which is slightly lighter than the dissolved δ^{56}Fe, and similar to earlier measurements of total particulate δ^{56}Fe on the East Siberian Arctic shelf (−0.2 ± 0.2‰; Conrad et al., 2018). Colloidal and leachable particulate δ^{56}Fe also appear not to be isotopically fractionated during transport from Siberian rivers to the North Pole in the TPD, again supporting that loss occurs by a non-fractionating process.

4.2. Fe in the Pacific Water Inflow

Below the Western Arctic surface mixed layer, modified Pacific water inflow forms a cold and nutrient rich upper halocline (Figure 3). Pacific waters carry high nutrient concentrations from the HNLC North Pacific, with additional nutrient and trace-metal contributions from the remineralization of organic matter in Bering and Chukchi shelf waters and porewaters, melting sea ice, and river waters (Aguilar-Islas et al., 2013; Cid et al., 2012; Kondo et al., 2016). Geochemical tracers such as N* and NO point to the intense remineralization and denitrification cycles on the shelves and in their porewaters (Alkire et al., 2019), and correlations to Ra isotopes suggest Fe, Mn, and Co concentrations over the shelves are predominantly controlled by reductive benthic fluxes (Kipp et al., 2019; Vieira et al., 2019).

Fe isotopes also provide strong evidence that the Fe found both over the continental shelves and in the halocline originates from reductive shelf sediments, based on the low δ^{56}Fe signatures which are typically associated with the input of Fe from reducing sediments (John et al., 2012, 2018; Severmann et al., 2010). Input from reducing sediments is apparent even at our GN01 station in the North Pacific (Station 1), where δ^{56}Fe between 249 to 733 m was −1.49‰ to −0.90‰, compared to −0.5‰ in intermediate waters in the central North East Pacific (Conway & John, 2015). This indicates Fe input from continental margins to intermediate North Pacific water depths, as previously reported based upon Fe concentration distributions across the North Pacific (Nishioka & Obata, 2017).

In the adjacent continental shelf waters, dFe concentrations are higher than in the North Pacific, with even lower δ^{56}Fe. The average dissolved δ^{56}Fe for all SHELF samples is −1.57 ± 0.66‰, which is much lower than other potential sources such as natural aerosols over the Arctic (−0.14–0.28‰) (Zhang et al., unpublished data; Gao et al., 2019), river runoff (−0.11 to 0.13‰; Escoube et al., 2015; Schroth et al., 2011), and melting sea ice (−0.36‰ to −1.10‰; Marsay et al., 2018), but is consistent with global observations of δ^{56}Fe input from reducing sediments where Fe(II) is released as a product of dissimilatory reduction (John et al., 2012, 2018; Severmann et al., 2010;). High Fe concentrations and low δ^{56}Fe are also found in the leachable particulate Fe phase above the shelf, roughly coincident with the region of high suspended particle concentration (Figures 3 and 4). Low light transmission has previously been attributed to both

biological particles from the surface and sediment resuspension (Uchimiya et al., 2016). Our Fe isotope data suggest that much of the labile particulate Fe originated as dissolved Fe(II) released from sediments and subsequently precipitated as iron oxyhydroxides.

4.3. Fe in the Atlantic Water Inflow

Below the Pacific inflow halocline, comprising most of the volume of the Arctic Ocean are the AW and DW water masses, which originate primarily as warm, salty water that flows into the Arctic through the Fram Strait (Woodgate, 2013). In contrast to the TPD and Pacific inflow, both of which show evidence of significant Fe inputs and biogeochemical cycling, neither Fe concentrations nor δ^{56}Fe in AW and DW (0.05 ± 0.30‰) appear to be significantly modified compared to values observed in intermediate waters of the subtropical North Atlantic, particularly for stations away from the continental margin (e.g., >82°N; Conway & John, 2014). A lack of Fe biogeochemical cycling might at first seem surprising, considering the long transport times and distances between the subtropical Atlantic and the Arctic, and the centuries-long residence time of waters within the deep Arctic (Schlosser et al., 1994). This highlights in part the lack of biological productivity in the surface central Arctic Ocean, and the consequent lack of significant biological material settling through the water column. While the continental shelves near the North Atlantic inflow have similar productivity compared to the Bering and Chukchi shelves (Sakshaug, 2004), they are deeper (~200 m), which may decrease the flux of organic matter to the sediments (e.g., Anderson et al., 2013; Jensen et al., 2019) and minimize Fe(II) production in sediment porewaters, thus explaining why Fe signatures do not show a similarly low δ^{56}Fe.

4.4. Sedimentary and Hydrothermal Fe Input in Arctic Deep Basin

While most of the deep Arctic has relatively homogeneous Fe concentrations and δ^{56}Fe similar to the Atlantic, distinct features are observed near the continental slopes and in the deep Amundsen Basin (Figures 3 and 4). Close to the continental slope, we observed high dFe with lower δ^{56}Fe, associated with high total suspended particle concentrations (Figures 3 and 4). Areas near continental shelves also had a relatively high concentration of labile particulate Fe and low lpδ^{56}Fe, though neither were the lpδ^{56}Fe concentrations as high, nor were the lpδ^{56}Fe values as low as those measured above the Bering Shelf. Nonetheless, the light δ^{56}Fe suggest an influence of Fe(II) from reducing sediment porewaters, even to deep waters. It is unlikely that this signal was produced *in situ* from the continental slope sediments, as productivity is much lower in the surface waters above the slope compared to those above the shelves, and slope sediments are not reducing (Gamboa et al., 2017; Goni et al., 2013). Instead, a possible source of this low-δ^{56}Fe Fe is downslope convection and entrainment driven by of high-salinity waters formed by brine-rejection during sea ice formation (Rudels, 2015). While we expect little redissolution of particulate sedimentary Fe under oxic conditions, there is a notably higher contribution of colloidal Fe to the dissolved phase near the slopes, suggesting that both the increased dFe and lower δ^{56}Fe might reflect the presence of additional isotopically-light colloidal Fe, while the δ^{56}Fe of the soluble phase may remain relatively unchanged.

Our single station that sampled the deep Amundsen Basin (Station 32, at the North Pole) was also unique, with elevated Fe concentrations, elevated concentrations of leachable particulate Fe, and higher δ^{56}Fe (Figure 4), which we tentatively attribute to hydrothermal Fe input with an apparent maximum around 2,400 m. Previous studies have described hydrothermal inputs to the deep Arctic from vents along the Gakkel Ridge (Edmonds et al., 2003), resulting in elevated 3He (Jean-Baptiste & Fourré, 2004), elevated dissolved Mn (Middag et al., 2011), and scavenging of thorium (Valk et al., 2018). Klunder, Laan, et al. (2012) previously observed a hydrothermal source of Fe from the Gakkel Ridge leading to a dFe maximum in the deep Amundsen Basin. The unique characteristics of Deep Water (DW) in the Amundsen Basin (Station 32) can be seen in comparison to DW in the Makarov Basin (Stations 30 and 38) which lies on the other side of the Lomonosov Ridge. Amundsen Basin dissolved Fe concentrations and δ^{56}Fe were both higher (0.41 ± 0.08 nmol kg^{-1} and 0.44 ± 0.18‰, n = 8) compared to the Makarov Basin (0.23 ± 0.04 nmol kg^{-1} and 0.23 ± 0.16‰, n = 12).

Hydrothermal fluids often have isotopically lighter Fe than continental material (Bennett et al., 2009; Conway & John, 2014; Rouxel et al., 2016; Severmann et al., 2004), but it is often observed that δ^{56}Fe increases

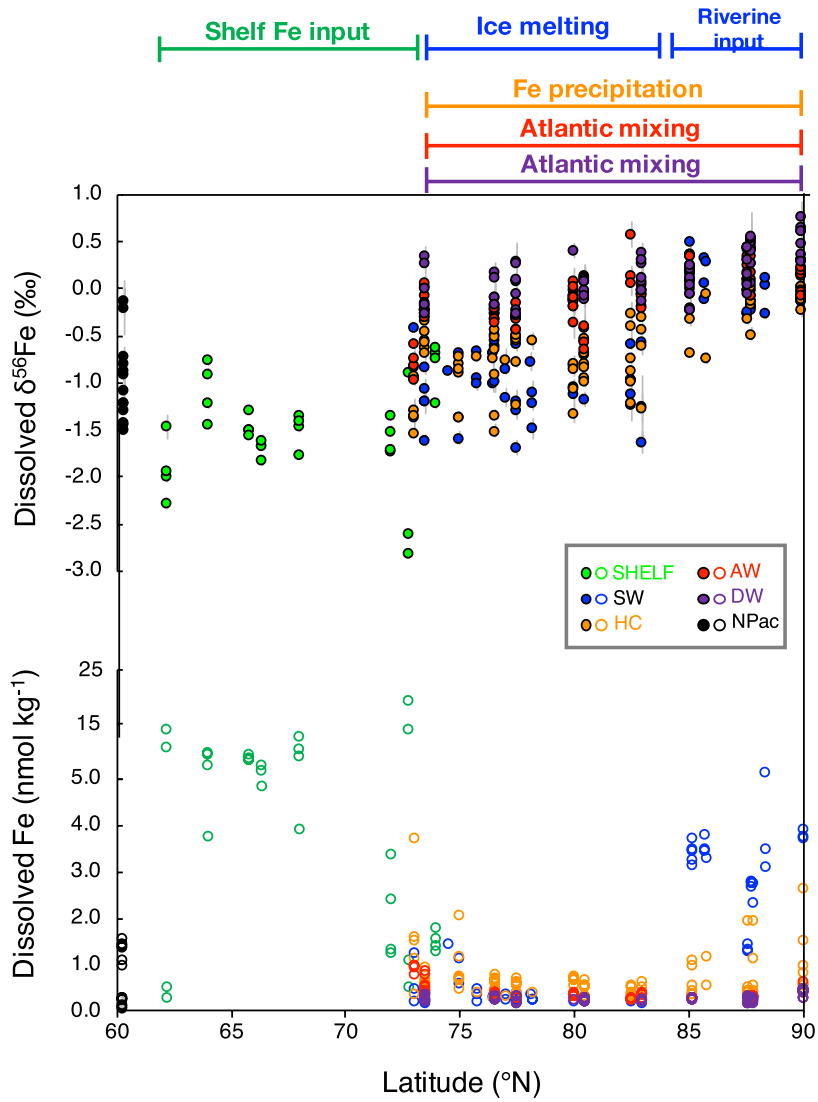

Figure 6. The basin-scale processes that cycle Fe in the Arctic Ocean include input from continental margin shelves, ice, melting, riverine input, precipitation, and input from the North Atlantic. These processes impact both Fe concentrations and δ^{56}Fe, as shown here for various water masses including waters over the continental shelves (SHELF), low-salinity surface waters, Pacific inflow halocline, Atlantic water, deep water, and the North Pacific.

as the plume moves away from the vent site (Conway & John,, 2014; Fitzsimmons et al., 2016, 2017; John et al., 2018; Klar et al., 2017), presumably from the persistence of a stable, isotopically heavy Fe phase bound by organic ligands (Dideriksen et al., 2008; Morgan et al., 2010). Indeed, the δ^{56}Fe values observed in the Makarov Basin are similar to the observations of heavy (+0.54 ± 0.14‰) hydrothermally sourced dissolved δ^{56}Fe values found >2,000 km east of the SEPR axis at ~25° S in the Peru/Chile Basin (Fitzsimmons et al., 2016) and thus may indicate a distal, stabilized dissolved Fe phase. Previous observations found organic Fe binding ligands of 1.98–2.05 nM over Gakkel Ridge (Thuróczy et al., 2011). However, because Gakkel Ridge hydrothermal fluids have not been measured for Fe isotopes to date, we cannot rule out a vent fluid source of heavy Fe to this region.

5. Conclusions

This first study of seawater Fe stable isotopes in the Arctic ocean highlights a variety of biogeochemical features along the GEOTRACES GN01 transect (Figure 6). For example, the shelf processes increase dFe concentrations and impart a light Fe isotope signature to North Pacific water flowing into the Arctic through

the Bering Shelf and Chukchi Shelf; δ^{56}Fe and dFe in Arctic SW reflect different Fe sources at various locations including a reducing sedimentary input near the shelves and an Asian riverine source in the transpolar drift. The relatively homogeneous dFe and δ^{56}Fe signals in deep Arctic waters reflect the lack of rapid Fe cycling in the deep Arctic. The Arctic is expected to undergo dramatic change as a result of global warming, leading to alterations in ice cover, biological productivity, and circulation (Barnhart et al., 2016; Krumpen et al., 2019; Nummelin et al., 2016; Post et al., 2013; Schourup-Kristensen et al., 2018; Walsh, 2008). As these changes occur, Fe may play a more important role in controlling Arctic productivity. Of course, the interactions between physical and biological processes in a changing Arctic are certain to be complex, and our data will therefore be a valuable baseline of comparison for future studies. Within this context, Fe stable isotopes may be a useful tool to understand contemporary Arctic biogeochemistry and to monitor future change.

Data Availability Statement

Data sets are available through the Biological and Chemical Oceanography Data Management Office (BCODMO; http://www.bco-dmo.org/project/638812).

Acknowledgments
The authors would like to thank the captain and crew of the USCGC *Healy* (HLY1502), as well as the chief scientists D. Kadko and W. Landing. The authors thank G. Weiss, S. Moos, and G. Cutter for seawater sampling, the Scripps ODF team for nutrient sampling and analysis, and Ana Aguilar-Islas and Robert Rember for collection of surface and ice hole samples. This work was founded by U.S. National Science Foundation grants OCE-1540254 to S. G. John, OCE-1713677 to J. N. Fitzsimmons and RMS, and OCE-1535854 to P. Lam. R. Zhang was also funded by the National Natural Science Foundation of China (41676175, 42076227) and Foundation for University Key Teacher by the Ministry of Education.

References

Abadie, C., Lacan, F., Radic, A., Pradoux, C., & Poitrasson, F. (2017). Iron isotopes reveal distinct dissolved iron sources and pathways in the intermediate versus deep Southern Ocean. *Proceedings of the National Academy of Sciences*, *114*, 858–863. https://doi.org/10.1073/pnas.1603107114

Aguilar-Islas, A. M., Rember, R., Nishino, S., Kikuchi, T., & Itoh, M. (2013). Partitioning and lateral transport of iron to the Canada Basin. *Polar Sciences*, *7*, 82–99. https://doi.org/10.1016/j.polar.2012.11.001

Aguilar-Islas, A. M., Rember, R. D., Mordy, C. W., & Wu, J. (2008). Sea ice-derived dissolved iron and its potential influence on the spring algal bloom in the Bering Sea. *Geophysical Research Letters*, *35*.

Alkire, M. B., Rember, R., & Polyakov, I. (2019). Discrepancy in the identification of the Atlantic/Pacific Front in the Central Arctic Ocean: NO versus nutrient relationships. *Geophysical Research Letters*, *46*, 3843–3852. https://doi.org/10.1029/2018GL081837

Anderson, L. G., Andersson, P. S., Björk, G., Peter Jones, E., Jutterström, S., & Wåhlström, I. (2013). Source and formation of the upper halocline of the Arctic Ocean. *Journal of Geophysical Research: Oceans*, *118*, 410–421. https://doi.org/10.1029/2012JC008291

Anderson, R. F. (2019). GEOTRACES: Accelerating research on the marine biogeochemical cycles of trace elements and their isotopes. *Annual Review of Marine Sciences*, *12*.

Ardiningsih, I., Krisch, S., Lodeiro, P., Reichart, G.-J., Achterberg, E. P., Gledhill, M., et al. (2020). Natural Fe-binding organic Ligands in Fram Strait and over the Northeast Greenland Shelf. *Marine Chemistry*, *224*, 103815. https://doi.org/10.1016/j.marchem.2020.103815

Barnhart, K. R., Miller, C. R., Overeem, I., & Kay, J. E. (2016). Mapping the future expansion of Arctic open water. *Nature Climate Change*, *6*, 280–285. https://doi.org/10.1038/nclimate2848

Beard, B. L., Johnson, C. M., Von Damm, K. L., & Poulson, R. L. (2003). Iron isotope constraints on Fe cycling and mass balance in oxygenated Earth oceans. *Geology*, *31*, 629. https://doi.org/10.1130/0091-7613(2003)031<0629:iicofc>2.0.co;2

Bennett, S. A., Rouxel, O., Schmidt, K., Garbe-Schönberg, D., Statham, P. J., & German, C. R. (2009). Iron isotope fractionation in a buoyant hydrothermal plume, 5 S Mid-Atlantic ridge. *Geochimica et Cosmochimica Acta*, *73*, 5619–5634. https://doi.org/10.1016/j.gca.2009.06.027

Bergquist, B. A., Wu, J., & Boyle, E. A. (2007). Variability in oceanic dissolved iron is dominated by the colloidal fraction. *Geochimica et Cosmochimica Acta*, *71*, 2960–2974. https://doi.org/10.1016/j.gca.2007.03.013

Berman-Frank, I., Quigg, A., Finkel, Z. V., Irwin, A. J., & Haramaty, L. (2007). Nitrogen-fixation strategies and Fe requirements in cyanobacteria. *Limnology & Oceanography*, *52*, 2260–2269. https://doi.org/10.4319/lo.2007.52.5.2260

Bishop, J. K. B., Lam, P. J., & Wood, T. J. (2012). Getting good particles: Accurate sampling of particles by large volume in-situ filtration. *Limnology and Oceanography: Methods*, *10*, 681–710. https://doi.org/10.4319/lom.2012.10.681

Boyd, P. W., & Ellwood, M. J. (2010). The biogeochemical cycle of iron in the ocean. *Nature Geoscience*, *3*, 675–682. https://doi.org/10.1038/ngeo964

Boyle, E. A., Edmond, J. M., & Sholkovitz, E. R. (1977). The mechanism of iron removal in estuaries. *Geochimica et Cosmochimica Acta*, *41*(9), 1977. https://doi.org/10.1016/0016-7037(77)90075-8

Bundy, R. M., Tagliabue, A., Hawco, N. J., Morton, P. L., Twining, B. S., Hatta, M., et al. (2020). Elevated sources of cobalt in the Arctic Ocean. *Biogeosciences*, *17*(19), 4745–4767. https://doi.org/10.5194/bg-17-4745-2020

Carmack, E. C. (2007). The alpha/beta ocean distinction: A perspective on freshwater fluxes, convection, nutrients and productivity in high-latitude seas. *Deep Sea Research Part II: Topical Studies in Oceanography*, *54*, 2578–2598. https://doi.org/10.1016/j.dsr2.2007.08.018

Charette, M. A., Kipp, L. E., Jensen, L. T., & others (2020). The transpolar drift as a source of riverine and shelf-derived trace elements to the Central Arctic Ocean. *Journal of Geophysical Research: Oceans*, e2019JC015920. https://doi.org/10.1029/2019JC015920

Cid, A. P., Nakatsuka, S., & Sohrin, Y. (2012). Stoichiometry among bioactive trace metals in the Chukchi and Beaufort Seas. *Journal of Oceanography*, *68*, 985–1001. https://doi.org/10.1007/s10872-012-0150-8

Conrad, S., Ingri, J., Gelting, J., Nordblad, F., Engström, E., Rodushkin, I., et al. (2018). Distribution of Fe isotopes in particles and colloids in the salinity gradient along the Lena River plume, Laptev Sea. *Biogeosciences*, 1–27. https://doi.org/10.5194/bg-2018-181

Conrad, S., Ingri, J., Gelting, J., Nordblad, F., Engström, E., Rodushkin, I., et al. (2019). Distribution of Fe isotopes in particles and colloids in the salinity gradient along the Lena River plume, Laptev Sea. *Biogeosciences*, *16*, 1305–1319. https://doi.org/10.5194/bg-16-1305-2019

Conway, T. M., & John, S. G. (2014). Quantification of dissolved iron sources to the North Atlantic Ocean. *Nature*, *511*, 212–215. https://doi.org/10.1038/nature13482

Conway, T. M., & John, S. G. (2015). The cycling of iron, zinc and cadmium in the North East Pacific Ocean—Insights from stable isotopes. *Geochimica et Cosmochimica Acta*, *164*, 262–283. https://doi.org/10.1016/j.gca.2015.05.023

Conway, T. M., Rosenberg, A. D., Adkins, J. F., & John, S. G. (2013). A new method for precise determination of iron, zinc and cadmium stable isotope ratios in seawater by double-spike mass spectrometry. *Analytica Chimica Acta*, *793*, 44–52. https://doi.org/10.1016/j.aca.2013.07.025

Cutter, G. A., & Bruland, K. W. (2012). Rapid and noncontaminating sampling system for trace elements in global ocean surveys. *Limnology and Oceanography: Methods*, *10*, 425–436. https://doi.org/10.4319/lom.2012.10.425

Dai, M. H., & Martin, J. M. (1995). First data on trace-metal level and behavior in 2 major Arctic River-estuarine systems (Ob and Yenisey) and in the adjacent Kara Sea, Russia. *Earth and Planetary Science Letters*, *131*(3–4), 127–141. https://doi.org/10.1016/0012-821x(95)00021-4

Dideriksen, K., Baker, J. A., & Stipp, S. L. S. (2008). Equilibrium Fe isotope fractionation between inorganic aqueous Fe (III) and the siderophore complex, Fe (III)-desferrioxamine B. *Earth and Planetary Science Letters*, *269*, 280–290. https://doi.org/10.1016/j.epsl.2008.02.022

Edmonds, H. N., Michael, P. J., Baker, E. T., Connelly, D. P., Snow, J. E., Langmuir, C. H., et al. (2003). Discovery of abundant hydrothermal venting on the ultraslow-spreading Gakkel ridge in the Arctic Ocean. *Nature*, *421*, 252–256. https://doi.org/10.1038/nature01351

Ellwood, M. J., Hutchins, D. A., Lohan, M. C., Milne, A., Nasemann, P., Nodder, S. D., et al. (2015). Iron stable isotopes track pelagic iron cycling during a subtropical phytoplankton bloom. *Proceedings of the National Academy of Sciences*, *112*, E15–E20. https://doi.org/10.1073/pnas.1421576112

Escoube, R., Rouxel, O. J., Pokrovsky, O. S., Schroth, A., Max Holmes, R., & Donard, O. F. X. (2015). Iron isotope systematics in Arctic rivers. *Comptes Rendus Geoscience*, *347*, 377–385. https://doi.org/10.1016/j.crte.2015.04.005

Evans, L. K., & Nishioka, J. (2018). Accumulation processes of trace metals into Arctic sea ice: Distribution of Fe, Mn and Cd associated with ice structure. *Marine Chemistry*.

Fitzsimmons, J. N., & Boyle, E. A. (2014). Assessment and comparison of Anopore and cross flow filtration methods for the determination of dissolved iron size fractionation into soluble and colloidal phases in seawater. *Limnology and Oceanography: Methods*, *12*, 246–263. https://doi.org/10.4319/lom.2014.12.246

Fitzsimmons, J. N., Carrasco, G. G., Wu, J., Roshan, S., Hatta, M., Measures, C. I., et al. (2015). Partitioning of dissolved iron and iron isotopes into soluble and colloidal phases along the GA03 GEOTRACES North Atlantic transect. *Deep Research Part II: Topical Studies in Oceanography*, *116*, 130–151. https://doi.org/10.1016/j.dsr2.2014.11.014

Fitzsimmons, J. N., Conway, T. M., Lee, J.-M., Kayser, R., Thyng, K. M., John, S. G., & Boyle, E. A. (2016). Dissolved iron and iron isotopes in the southeastern Pacific Ocean. *Global Biogeochemical Cycles*, *30*, 1372–1395. https://doi.org/10.1002/2015GB005357

Fitzsimmons, J. N., Hayes, C. T., Al-Subiai, S. N., Zhang, R., Morton, P. L., Weisend, R. E., et al. (2015). Daily to decadal variability of size-fractionated iron and iron-binding ligands at the Hawaii ocean time-series station ALOHA. *Geochimica et Cosmochimica Acta*, *171*, 303–324. https://doi.org/10.1016/j.gca.2015.08.012

Fitzsimmons, J. N., John, S. G., Marsay, C. M., Hoffman, C. L., Nicholas, S. L., Toner, B. M., et al. (2017). Iron persistence in a distal hydrothermal plume supported by dissolved-particulate exchange. *Nature Geoscience*, *10*, 195–201. https://doi.org/10.1038/ngeo2900

Gamboa, A., Montero-Serrano, J.-C., St-Onge, G., Rochon, A., & Desiage, P.-A. (2017). Mineralogical, geochemical, and magnetic signatures of surface sediments from the Canadian Beaufort Shelf and Amundsen Gulf (Canadian Arctic). *Geochemistry, Geophysics, Geosystems*, *18*(2), 488–512. https://doi.org/10.1002/2016GC006477

Gao, Y., Marsay, C. M., Yu, S., Fan, S., Mukherjee, P., Buck, C. S., & Landing, W. M. (2019). Particle-size variability of aerosol iron and impact on iron solubility and dry deposition fluxes to the Arctic Ocean. *Scientific Reports*, *9*, 16653. https://doi.org/10.1038/s41598-019-52468-z

Goni, M. A., O'Connor, A. E., Kuzyk, Z. Z., Yunker, M. B., Gobeil, C., & Macdonald, R. W. (2013). Distribution and sources of organic matter in surface marine sediments across the North American Arctic margin. *Journal of Geophysical Research: Oceans*, *118*, 4017–4035. https://doi.org/10.1002/jgrc.20286

Granger, J., Sigman, D. M., Gagnon, J., Tremblay, J.-E., & Mucci, A. (2018). On the properties of the Arctic halocline and deep water masses of the Canada Basin from nitrate isotope ratios. *Journal of Geophysical Research: Oceans*, *123*, 5443–5458. https://doi.org/10.1029/2018JC014110

Guay, C. K., & Kenison Falkner, K. (1997). Barium as a tracer of Arctic halocline and river waters. *Deep Sea Research Part II: Topical Studies in Oceanography*, *44*, 1543–1569. https://doi.org/10.1016/S0967-0645(97)00066-0

Harding, K., Turk-Kubo, K. A., Sipler, R. E., Mills, M. M., Bronk, D. A., & Zehr, J. P. (2018). Symbiotic unicellular cyanobacteria fix nitrogen in the Arctic Ocean. *Proceedings of the National Academy of Sciences*, *115*, 13371–13375. https://doi.org/10.1073/pnas.1813658115

Hein, J. R., Konstantinova, N., Mikesell, M., Mizell, K., Fitzsimmons, J. N., Lam, P. J., et al. (2017). Arctic deep water ferromanganese-oxide deposits reflect the unique characteristics of the Arctic Ocean. *Geochemistry, Geophysics, Geosystems*, *18*, 3771–3800. https://doi.org/10.1002/2017GC007186

Hioki, N., Kuma, K., Morita, Y., Sasayama, R., Ooki, A., Kondo, Y., et al. (2014). Laterally spreading iron, humic-like dissolved organic matter and nutrients in cold, dense subsurface water of the Arctic Ocean. *Scientific Reports*, *4*, 6775. https://doi.org/10.1038/srep06775

Hirst, C., Andersson, P. S., Kooijman, E., Schmitt, M., Kutscher, L., Maximov, T., et al. (2020). Iron isotopes reveal the sources of Fe-bearing particles and colloids in the Lena River basin. *Geochimica et Cosmochimica Acta*, *269*, 678–692. https://doi.org/10.1016/j.gca.2019.11.004

Holmes, R. M., McClelland, J. W., Peterson, B. J., Tank, S. E., Bulygina, E., Eglinton, T. I., et al. (2012). Seasonal and annual fluxes of nutrients and organic matter from large rivers to the Arctic ocean and surrounding seas. *Estuaries and Coasts*, *35*, 369–382. https://doi.org/10.1007/s12237-011-9386-6

Hopwood, M. J., Cantoni, C., Clarke, J. S., Cozzi, S., & Achterberg, E. P. (2017). The heterogeneous nature of Fe delivery from melting icebergs. *Geochemical Perspectives Letters*, *3*, 200–209. https://doi.org/10.7185/geochemlet.1723

Jean-Baptiste, P., & Fourré, E. (2004). Hydrothermal activity on Gakkel Ridge. *Nature*, *428*, 36–36. https://doi.org/10.1038/428036a

Jensen, L. T., Morton, P., Twining, B. S., Heller, M. I., Hatta, M., Measures, C. I., et al. (2020). A comparison of marine Fe and Mn cycling: U.S. GEOTRACES GN01 Western Arctic case study. *Geochimica et Cosmochimica Acta*, *288*, 138–160. https://doi.org/10.1016/j.gca.2020.08.006

Jensen, L. T., Wyatt, N. J., Landing, W. M., & Fitzsimmons, J. N. (2020). Assessment of the stability, sorption, and exchangeability of marine dissolved and colloidal metals. *Marine Chemistry*, *220*, 103754. https://doi.org/10.1016/j.marchem.2020.103754

Jensen, L. T., Wyatt, N. J., Twining, B. S., Rauschenberg, S., Landing, W. M., Sherrell, R. M., & Fitzsimmons, J. N. (2019). Biogeochemical cycling of dissolved zinc in the Western Arctic (Arctic GEOTRACES GN01). *Global Biogeochemical Cycles*, *33*, 343–369. https://doi.org/10.1029/2018gb005975

John, S. G., Helgoe, J., Townsend, E., Weber, T., DeVries, T., Tagliabue, A., et al. (2018). Biogeochemical cycling of Fe and Fe stable isotopes in the Eastern Tropical South Pacific. *Marine Chemistry*, *201*, 66–76. https://doi.org/10.1016/j.marchem.2017.06.003

John, S. G., Mendez, J., Moffett, J., & Adkins, J. (2012). The flux of iron and iron isotopes from San Pedro Basin sediments. *Geochimica et Cosmochimica Acta*, *93*, 14–29. https://doi.org/10.1016/j.gca.2012.06.003

Kadko, D., Aguilar-Islas, A., Bolt, C., Buck, C. S., Fitzsimmons, J. N., Jensen, L. T., et al. (2019). The residence times of trace elements determined in the surface Arctic Ocean during the 2015 US Arctic GEOTRACES expedition. *Marine Chemistry*, *208*, 56–69. https://doi.org/10.1016/j.marchem.2018.10.011

Kipp, L. E., Charette, M. A., Moore, W. S., Henderson, P. B., & Rigor, I. G. (2018). Increased fluxes of shelf-derived materials to the central Arctic Ocean. *Science Advances*, *4*, eaao1302. https://doi.org/10.1126/sciadv.aao1302

Kipp, L. E., Kadko, D. C., Pickart, R. S., Henderson, P. B., Moore, W. S., & Charette, M. A. (2019). Shelf-basin interactions and water mass residence times in the Western Arctic ocean: Insights provided by radium isotopes. *Journal of Geophysical Research: Oceans*, *124*, 3279–3297. https://doi.org/10.1029/2019JC014988

Klar, J. K., James, R. H., Gibbs, D., Lough, A., Parkinson, I., Milton, J. A., et al. (2017). Isotopic signature of dissolved iron delivered to the Southern Ocean from hydrothermal vents in the East Scotia Sea. *Geology*, *45*, 351–354. https://doi.org/10.1130/G38432.1

Klunder, M. B., Bauch, D., Laan, P., De Baar, H. J., van Heuven, S., & Ober, S. (2012). Dissolved iron in the Arctic shelf seas and surface waters of the central Arctic Ocean: Impact of Arctic river water and ice-melt. *Journal of Geophysical Research: Oceans*, *117*, 1–18. https://doi.org/10.1029/2011JC007133

Klunder, M. B., Laan, P., Middag, R., De Baar, H. J., & Bakker, K. (2012). Dissolved iron in the Arctic Ocean: Important role of hydrothermal sources, shelf input and scavenging removal. *Journal of Geophysical Research: Oceans*, *117*. https://doi.org/10.1029/2011jc007135

Kondo, Y., Obata, H., Hioki, N., Ooki, A., Nishino, S., Kikuchi, T., & Kuma, K. (2016). Transport of trace metals (Mn, Fe, Ni, Zn and Cd) in the western Arctic Ocean (Chukchi Sea and Canada Basin) in late summer 2012. *Deep-Sea Research Part I: Oceanographic Research Papers*, *116*, 236–252. https://doi.org/10.1016/j.dsr.2016.08.010

Krisch, S., Browning, T. J., Graeve, M., Ludwichowski, K.-U., Lodeiro, P., Hopwood, M. J., et al. (2020). The influence of Arctic Fe and Atlantic fixed N on summertime primary production in Fram Strait, North Greenland Sea. *Scientific Reports*, *10*(1), 15230. https://doi.org/10.1038/s41598-020-72100-9

Krumpen, T., Belter, H. J., Boetius, A., Damm, E., Haas, C., Hendricks, S., et al. (2019). Arctic warming interrupts the transpolar drift and affects long-range transport of sea ice and ice-rafted matter. *Scientific Reports*, *9*, 5459. https://doi.org/10.1038/s41598-019-41456-y

Labatut, M., Lacan, F., Pradoux, C., Chmeleff, J., Radic, A., Murray, J. W., et al. (2014). Iron sources and dissolved-particulate interactions in the seawater of the Western Equatorial Pacific, iron isotope perspectives. *Global Biogeochemical Cycles*, *28*, 1044–1065. https://doi.org/10.1002/2014GB004928

Laglera, L. M., Sukekava, C., Slagter, H. A., Downes, J., Aparicio-Gonzalez, A., & Gerringa, L. J. A. (2019). First quantification of the controlling role of humic substances in the transport of iron across the surface of the Arctic Ocean. *Environmental Science and Technology*, *53*, 13136–13145. https://doi.org/10.1021/acs.est.9b04240

Lam, P. J., Lee, J.-M., Heller, M. I., Mehic, S., Xiang, Y., & Bates, N. R. (2018). Size-fractionated distributions of suspended particle concentration and major phase composition from the U.S. GEOTRACES Eastern Pacific Zonal Transect (GP16). *Marine Chemistry*, *201*, 90–107. https://doi.org/10.1016/j.marchem.2017.08.013

Lee, J.-M., Heller, M. I., & Lam, P. J. (2018). Size distribution of particulate trace elements in the U.S. GEOTRACES Eastern Pacific Zonal Transect (GP16). *Marine Chemistry*, *201*, 108–123. https://doi.org/10.1016/j.marchem.2017.09.006

Lewis, K. M., Arntsen, A. E., Coupel, P., Joy-Warren, H., Lowry, K. E., Matsuoka, A., et al. (2019). Photoacclimation of Arctic Ocean phytoplankton to shifting light and nutrient limitation. *Limnology & Oceanography*, *64*, 284–301. https://doi.org/10.1002/lno.11039

Manizza, M., Menemenlis, D., Zhang, H., & Miller, C. E. (2019). Modeling the recent changes in the Arctic Ocean CO_2 sink (2006–2013). *Global Biogeochemical Cycles*, *33*, 420–438. https://doi.org/10.1029/2018GB006070

Marsay, C. M., Aguilar-Islas, A., Fitzsimmons, J. N., Hatta, M., Jensen, L. T., John, S. G., et al. (2018). Dissolved and particulate trace elements in late summer Arctic melt ponds. *Marine Chemistry*, *204*, 70–85. https://doi.org/10.1016/j.marchem.2018.06.002

Martin, J. H. (1990). Glacial-interglacial CO_2 change: The iron hypothesis. *Paleoceanography*, *5*, 1–13. https://doi.org/10.1029/pa005i001p00001

Measures, C. I. (1999). The role of entrained sediments in sea ice in the distribution of aluminium and iron in the surface waters of the Arctic Ocean. *Marine Chemistry*, *68*(1–2), 59–70. https://doi.org/10.1016/S0304-4203(99)00065-1

Middag, R., de Baar, H. J. W., Laan, P., & Klunder, M. B. (2011). Fluvial and hydrothermal input of manganese into the Arctic Ocean. *Geochimica et Cosmochimica Acta*, *75*, 2393–2408. https://doi.org/10.1016/j.gca.2011.02.011

Moore, J. K., Doney, S. C., Glover, D. M., & Fung, I. Y. (2002). Iron cycling and nutrient-limitation patterns in surface waters of the World Ocean. *Deep Research Part II-Topical Studies in Oceanography*, *49*, 463–507. https://doi.org/10.1016/S0967-0645(01)00109-6

Morgan, J. L. L., Wasylenki, L. E., Nuester, J., & Anbar, A. D. (2010). Fe isotope fractionation during equilibration of Fe−organic complexes. *Environmental Science and Technology*, *44*, 6095–6101. https://doi.org/10.1021/es100906z

Nishioka, J., & Obata, H. (2017). Dissolved iron distribution in the western and central subarctic Pacific: HNLC water formation and biogeochemical processes. *Limnology & Oceanography*, *62*, 2004–2022. https://doi.org/10.1002/lno.10548

Nummelin, A., Ilicak, M., Li, C., & Smedsrud, L. H. (2016). Consequences of future increased Arctic runoff on Arctic Ocean stratification, circulation, and sea ice cover. *Journal of Geophysical Research: Oceans*, *121*, 617–637. https://doi.org/10.1002/2015JC011156

Ohnemus, D. C., Auro, M. E., Sherrell, R. M., Lagerström, M., Morton, P. L., Twining, B. S., et al. (2014). Laboratory intercomparison of marine particulate digestions including Piranha: A novel chemical method for dissolution of polyethersulfone filters. *Limnology and Oceanography: Methods*, *12*, 530–547. https://doi.org/10.4319/lom.2014.12.530

Ohnemus, D. C., & Lam, P. J. (2015). Cycling of lithogenic marine particles in the US GEOTRACES North Atlantic transect. *Deep Research Part II: Topical Studies in Oceanography*, *116*, 283–302. https://doi.org/10.1016/j.dsr2.2014.11.019

Overland, J., Dunlea, E., Box, J. E., Corell, R., Forsius, M., Kattsov, V., et al. (2019). The urgency of Arctic change. *Polar Sciences*, *21*, 6–13. https://doi.org/10.1016/j.polar.2018.11.008

Planquette, H., & Sherrell, R. M. (2012). Sampling for particulate trace element determination using water sampling bottles: Methodology and comparison to in situ pumps. *Limnology and Oceanography: Methods*, *10*, 367–388. https://doi.org/10.4319/lom.2012.10.367

Post, E., Bhatt, U. S., Bitz, C. M., Brodie, J. F., Fulton, T. L., Hebblewhite, M., et al. (2013). Ecological consequences of sea-ice decline. *Science*, *341*, 519–524. https://doi.org/10.1126/science.1235225

Radic, A., Lacan, F., & Murray, J. W. (2011). Iron isotopes in the seawater of the equatorial Pacific Ocean: New constraints for the oceanic iron cycle. *Earth and Planetary Science Letters*, *306*, 1–10. https://doi.org/10.1016/j.epsl.2011.03.015

Randelhoff, A., Holding, J., Janout, M., Sejr, M. K., Babin, M., Tremblay, J. É., & Alkire, M. B. (2020). Pan-Arctic ocean primary production constrained by turbulent nitrate fluxes. *Frontiers in Marine Sciences*, *7*. https://doi.org/10.3389/fmars.2020.00150

Revels, B. N., Zhang, R., Adkins, J. F., & John, S. G. (2015). Fractionation of iron isotopes during leaching of natural particles by acidic and circumneutral leaches and development of an optimal leach for marine particulate iron isotopes. *Geochimica et Cosmochimica Acta*, *166*, 92–104. https://doi.org/10.1016/j.gca.2015.05.034

Rijkenberg, M. J. A., Slagter, H. A., Rutgers van der Loeff, M., van Ooijen, J., & Gerringa, L. J. A. (2018). Dissolved Fe in the deep and upper Arctic ocean with a focus on Fe limitation in the Nansen Basin. *Frontiers in Marine Sciences*, *5*, 1–14. https://doi.org/10.3389/fmars.2018.00088

Rouxel, O., Toner, B. M., Manganini, S. J., & German, C. R. (2016). Geochemistry and iron isotope systematics of hydrothermal plume fallout at East Pacific Rise 9°50′N. *Chemical Geology*, *441*, 212–234. https://doi.org/10.1016/j.chemgeo.2016.08.027

Rudels, B. (2015). Arctic Ocean circulation, processes and water masses: A description of observations and ideas with focus on the period prior to the International Polar Year 2007–2009. *Progress in Oceanography*, *132*, 22–67. https://doi.org/10.1016/j.pocean.2013.11.006

Rudels, B., Larsson, A.-M., & Sehlstedt, P.-I. (1991). Stratification and water mass formation in the Arctic Ocean: Some implications for the nutrient distribution. *Polar Research*, *10*(1), 19–32. https://doi.org/10.1111/j.1751-8369.1991.tb00631.x

Rutgers van der Loeff, M., Kipp, L., Charette, M. A., Moore, W. S., Black, E., Stimac, I., et al. (2018). Radium isotopes across the Arctic Ocean show time scales of water mass ventilation and increasing shelf inputs. *Journal of Geophysical Research: Oceans*, *123*, 4853–4873. https://doi.org/10.1029/2018JC013888

Sakshaug, E. (2004). Primary and secondary production in the Arctic Seas. In *The organic carbon cycle in the Arctic Ocean* (pp. 57–81). Springer. https://doi.org/10.1007/978-3-642-18912-8_3

Schlosser, P., Kromer, B., Östlund, G., Ekwurzel, B., Bönisch, G., Loosli, H. H., & Purtschert, R. (1994). On the ^{14}C and ^{39}Ar distribution in the Central Arctic Ocean: Implications for deep water formation. *Radiocarbon*, *36*, 327–343. https://doi.org/10.1017/S003382220001451X

Schourup-Kristensen, V., Wekerle, C., Wolf-Gladrow, D. A., & Völker, C. (2018). Arctic Ocean biogeochemistry in the high resolution FESOM 1.4-REcoM2 model. *Progress in Oceanography*, *168*, 65–81. https://doi.org/10.1016/j.pocean.2018.09.006

Schroth, A. W., Crusius, J., Chever, F., Bostick, B. C., & Rouxel, O. J. (2011). Glacial influence on the geochemistry of riverine iron fluxes to the Gulf of Alaska and effects of deglaciation. *Geophysical Research Letters*, *38*. https://doi.org/10.1029/2011GL048367

Severmann, S., Johnson, C. M., Beard, B. L., German, C. R., Edmonds, H. N., Chiba, H., & Green, D. R. H. (2004). The effect of plume processes on the Fe isotope composition of hydrothermally derived Fe in the deep ocean as inferred from the Rainbow vent site, Mid-Atlantic Ridge, 36 14′N. *Earth and Planetary Science Letters*, *225*, 63–76. https://doi.org/10.1016/j.epsl.2004.06.001

Severmann, S., McManus, J., Berelson, W. M., & Hammond, D. E. (2010). The continental shelf benthic iron flux and its isotope composition. *Geochimica et Cosmochimica Acta*, *74*, 3984–4004. https://doi.org/10.1016/j.gca.2010.04.022

Shen, Y., Benner, R., Robbins, L. L., & Wynn, J. G. (2016). Sources, distributions, and dynamics of dissolved organic matter in the Canada and Makarov Basins. *Frontiers in Marine Sciences*, *3*, 198. https://doi.org/10.3389/fmars.2016.00198

Sipler, R. E., Gong, D., Baer, S. E., Sanderson, M. P., Roberts, Q. N., Mulholland, M. R., & Bronk, D. A. (2017). Preliminary estimates of the contribution of Arctic nitrogen fixation to the global nitrogen budget. *Limnology and Oceanography Letters*, *2*, 159–166. https://doi.org/10.1002/lol2.10046

Slagter, H. A., Laglera, L. M., Sukekava, C., & Gerringa, L. J. A. (2019). Fe-binding organic ligands in the humic-rich transpolar drift in the surface Arctic Ocean using multiple voltammetric methods. *Journal of Geophysical Research: Oceans*, *124*, 1491–1508. https://doi.org/10.1029/2018JC014576

Slagter, H. A., Reader, H. E., Rijkenberg, M. J. A., Rutgers van der Loeff, M., de Baar, H. J. W., & Gerringa, L. J. A. (2017). Organic Fe speciation in the Eurasian Basins of the Arctic Ocean and its relation to terrestrial DOM. *Marine Chemistry*, *197*, 11–25. https://doi.org/10.1016/j.marchem.2017.10.005

Stevenson, E. I., Fantle, M. S., Das, S. B., Williams, H. M., & Aciego, S. M. (2017). The iron isotopic composition of subglacial streams draining the Greenland ice sheet. *Geochimica et Cosmochimica Acta*, *213*, 237–254. https://doi.org/10.1016/j.gca.2017.06.002

Tagliabue, A., Bowie, A. R., Boyd, P. W., Buck, K. N., Johnson, K. S., & Saito, M. A. (2017). The integral role of iron in ocean biogeochemistry. *Nature*, *543*, 51–59. https://doi.org/10.1038/nature21058

Taylor, R. L., Semeniuk, D. M., Payne, C. D., Zhou, J., Tremblay, J. É., Cullen, J. T., & Maldonado, M. T. (2013). Colimitation by light, nitrate, and iron in the Beaufort Sea in late summer. *Journal of Geophysical Research: Oceans*, *118*(7), 3260–3277. https://doi.org/10.1002/jgrc.20244

Thuróczy, C., Gerringa, L. J. A., Klunder, M., Laan, P., Le Guitton, M., & De Baar, H. J. W. (2011). Distinct trends in the speciation of iron between the shallow shelf seas and the deep basins of the Arctic Ocean. *Journal of Geophysical Research: Oceans*, *116*. https://doi.org/10.1029/2010jc006835

Uchimiya, M., Motegi, C., Nishino, S., Kawaguchi, Y., Inoue, J., Ogawa, H., & Nagata, T. (2016). Coupled response of bacterial production to a wind-induced fall phytoplankton bloom and sediment resuspension in the Chukchi sea shelf, Western Arctic Ocean. *Frontiers in Marine Science*, *3*, 231. https://doi.org/10.3389/fmars.2016.00231

Valk, O., Rutgers van der Loeff, M. M., & Geibert, W. (2018). Importance of hydrothermal vents in scavenging removal of 230Th in the Nansen Basin. *Geophysical Research Letters*, *45*, 10–539. https://doi.org/10.1029/2018gl079829

Vieira, L. H., Achterberg, E. P., Scholten, J., Beck, A. J., Liebetrau, V., Mills, M. M., & Arrigo, K. R. (2019). Benthic fluxes of trace metals in the Chukchi Sea and their transport into the Arctic Ocean. *Marine Chemistry*, *208*, 43–55. https://doi.org/10.1016/j.marchem.2018.11.001

Walsh, J. E. (2008). Climate of the Arctic marine environment. *Ecological Applications*, *18*, S3–S22. https://doi.org/10.1890/06-0503.1

Whitmore, L. M., Morton, P. L., Twining, B. S., & Shiller, A. M. (2019). Vanadium cycling in the Western Arctic Ocean is influenced by shelf-basin connectivity. *Marine Chemistry*, *216*, 103701. https://doi.org/10.1016/j.marchem.2019.103701

Woodgate, R. (2013). Arctic ocean circulation: Going around at the top of the world. *Nature Education Knowledge*, *4*, 8.

Xiang, Y., & Lam, P. J. (2020). Size-fractionated marine suspended particle dynamics in the Western Arctic Ocean from the U.S. GEOTRACES Arctic cruise (GN01). *Journal of Geophysical Research: Oceans*, *125*(8), e2020JC016144. https://doi.org/10.1029/2020jc016144

Zhang, R., Jensen, L. T., Fitzsimmons, J. N., Sherrell, R. M., & John, S. (2019). Dissolved cadmium and cadmium stable isotopes in the western Arctic Ocean. *Geochimica Cosmochimica Acta*, *258*, 258–273. https://doi.org/10.1016/j.gca.2019.05.028

Zhang, R., John, S. G., Zhang, J., Ren, J., Wu, Y., Zhu, Z., et al. (2015). Transport and reaction of iron and iron stable isotopes in glacial meltwaters on Svalbard near Kongsfjorden: From rivers to estuary to ocean. *Earth and Planetary Science Letters*, *424*, 201–211. https://doi.org/10.1016/j.epsl.2015.05.031